Design of a high temperature falling bed air preheater for direct coal-fired MHD power generation using liquid slag droplets
by Raymond Lee Prill

A thesis submitted in partial fulfillment of the requirements for the degree of MASTER OF SCIENCE in Mechanical Engineering
Montana State University

Abstract:
A unique design for a falling liquid droplet heat exchanger is presented. The major problem associated with this type of heat exchanger, that of obtaining uniformly sized liquid droplets, has been solved by utilizing vibration induced atomization of the liquid. With this method the drops are formed by disturbing a liquid capillary jet by either vibrating a distributor plate through which the liquid flows or by holding the plate stationary and producing the disturbance with external sound pressure waves. Specific use of this type of heat exchanger as a direct coal fired air preheater for MHD power generation is examined. Digital solution of the governing equations has determined the effect of particle size and size distribution on the chamber size requirement. Comparisons with other MHD preheater design concepts, including the cored brick, show the present design has numerous advantages.

STATEMENT OF PERMISSION TO COPY

In presenting this thesis in partial fulfillment of the requirements for an advanced degree at Montana State University, I agree that the Library shall make it freely available for inspection. I further agree that permission for extensive copying of this thesis for scholarly purposes may be granted by my major professor, or, in his absence, by the Director of Libraries. It is understood that any copying or publication of this thesis for financial gain shall not be allowed without my written permission.

Signature Raymond L Pill

Date May 18, 1977

DESIGN OF A HIGH TEMPERATURE FALLING BED AIR PREHEATER FOR DIRECT COAL-FIRED MHD POWER GENERATION USING LIQUID SLAG DROPLETS

by

RAYMOND LEE PRILL

A thesis submitted in partial fulfillment
of the requirements for the degree

of

MASTER OF SCIENCE

in

Mechanical Engineering

Approved:

Ronald Mussulman
Chairperson, Graduate Committee

D.O. Blackketter by RC Challender
Head, Major Department

Henry L Parsons
Graduate Dean

MONTANA STATE UNIVERSITY
Bozeman, Montana

May, 1977

ACKNOWLEDGMENTS

The author wishes to thank Dr. R. Mussulman for his guidance and instruction during the course of this project. Special thanks also goes to Dr. R. Warrington for his suggestions and encouragement. The writer also thanks Dr. W. Genetti for his assistance.

This study was supported by ERDA/MHD Division and the Mechanical Engineering Department of Montana State University.

TABLE OF CONTENTS

TABLE OF CONTENTS (cont)

LIST OF TABLES

LIST OF FIGURES

NOMENCLATURE

SYMBOL	DESCRIPTION
a	acceleration of gravity
a_r	Rosseland absorption coefficient
c	specific heat
d	droplet diameter
f	shadowing factor or frequency function
h	heat transfer coefficient
i_b	black body radiative intensity
k	thermal conductivity
ℓ	length
$\dot{m}$	mass flow rate
n	droplet number density
q	heat flux (per unit area and time)
r	radius
s_d	standard deviation
t	time
x	distance from the top of the chamber
A	area
C_D	drag coefficient
D	diameter
F	frequency
Gr	Grashof number

SYMBOL	DESCRIPTION
H	overall heat transfer coefficient
L	chamber length
N	total number of descrete sizes of droplets
Nu	Nusselt number
P	chamber pressure
Pr	Prandtl number
Qr	radiative heat transfer rate
Qcov	convective heat transfer rate
R	gas constant or radius
Re	Reynolds number
T	temperature
T_1	temperature at top of upper chamber
T_2	temperature at bottom of upper chamber
T_3	temperature at top of lower chamber
T_4	temperature at bottom of lower chamber
U	dimensionless velocity parameter
V	velocity
V_1	velocity at top of upper chamber
V_2	velocity at bottom of upper chamber
V_3	velocity at top of lower chamber
V_4	velocity at bottom of lower chamber

SYMBOL	DESCRIPTION
α	absorption coefficient
β	volume coefficient of expansion
η	dimensionless distance
ϕ	dimensionless temperature parameter
μ	dynamic viscosity
ρ	density
σ	Stefan-Boltzmann constant
σ_s	surface tension
Ω	solid angle
ψ	dimensionless quantity characterizing heat transfer chamber requirements

SUBSCRIPTS

a	air
c	capillary
g	gas
in	inner
j	jet
m	mean
max	maximum
min	minimum
o	outer

SYMBOL	DESCRIPTION
opt	optimum
r	relative or radiative
s	slag
term	terminal
w	wall

SUPERSCRIPTS

'	derivative
*	dimensionless quantity

ABSTRACT

A unique design for a falling liquid droplet heat exchanger is presented. The major problem associated with this type of heat exchanger, that of obtaining uniformly sized liquid droplets, has been solved by utilizing vibration induced atomization of the liquid. With this method the drops are formed by disturbing a liquid capillary jet by either vibrating a distributor plate through which the liquid flows or by holding the plate stationary and producing the disturbance with external sound pressure waves. Specific use of this type of heat exchanger as a direct coal fired air preheater for MHD power generation is examined. Digital solution of the governing equations has determined the effect of particle size and size distribution on the chamber size requirement. Comparisons with other MHD preheater design concepts, including the cored brick, show the present design has numerous advantages.

CHAPTER I

INTRODUCTION

The efficiency of a fossil fueled open cycle magnetohydrodynamic power generating plant depends strongly on the temperature of the working gas. The required combustion temperatures, on the order of 3000K, can be achieved by either preheating the combustion air to a high temperature, around 2000K, or by use of oxygen enriched air. Because of the amount of oxygen that would be needed in a large scale MHD power plant, the latter of these methods was not considered in this study.

There are two basic types of air preheaters for open cycle MHD applications - the directly fired and indirectly fired. The directly fired preheater utilizes the thermal energy of the exhaust gas from the MHD channel to preheat the air while the indirectly fired facility uses the exhaust gas from a separately fired, clean fuel combuster. The indirectly fired preheater, though not having to withstand the deleterious properties of the fly ash slag, sulfur, and potassium seed contained in an MHD exhaust gas, would require an expensive clean burning fuel such as natural gas and would lower the overall plant efficiency. Therefore, the full exploitation of the efficiency advantages of an MHD power plant is dependent on the employment of high temperature directly fired air preheaters.

Four types of preheater designs have in the past been considered for coal fired MHD applications:

1) the chequerwork packed bed preheater
2) the packed pebble bed preheater
3) the cored brick packed bed preheater
4) the falling bed preheater

All of these are regenerative type heat exchangers.

Polish researchers have sized the chequerwork type preheater and found the dimensions quite large (1). Creep of the ceramic bricks at the bottom of such a massive chequerwork is a serious problem. The packed pebble bed type preheaters have the inherent problem of plugging up from the coal slag deposits, though they are feasible in an indirectly fired facility (2). The cored brick preheater offers both the possibility of not plugging from the exhaust gas coal slag deposits and good thermal effectiveness (3).

All packed bed type preheaters (chequerwork, pebble bed and cored brick) operate in a cyclic mode of heat-up and blow-down. This requires large gas valves in the MHD exhaust gas flow stream operating periodically and sealing against the differential pressure between the inlet and outlet of the MHD channel (approximately 7 atmospheres) at high temperatures (around 2000K). These valves represent large capital costs and raise serious reliability questions. This problem, teamed with the problems of finding a durable bed material and reducing plugging and fouling to an acceptable level, has caused preheater design to lag behind development of other MHD components.

The falling bed concept represents one solution to the problems of other directly fired MHD preheater design concepts. This design employs heat transfer from particles falling through a counterflow of gas. In the MHD application the particles would be heated in one set of chambers by the exhaust from the MHD channel. These heated particles would then fall through a counterflow of combustion air in a second chamber. Figure 1.1 shows the flow process involved. Continuous recycling of the bed materials eliminates any valves in the exhaust gas flow. The large surface-area-to-mass ratio of the particles in the falling bed preheater give it potential for high heat transfer rates.

Two types of bed material for the falling particle preheater have been proposed; solid particles of a material like alumina (4, 5) and liquid droplets of a material like coal slag. Extensive research was done on the atomization of liquid slag by a team of English engineers (6). These studies were focused on the use of twin jet atomizers, breaking up a jet of liquid slag with a jet of air. This type of atomizer had the disadvantage of a wide dispersion of droplet sizes, causing large chamber length requirements.

If the droplets are mono-disperse in size, they can be partially "floated" by the gas and the chambers can be very compact. As the droplet size dispersion increases the velocity of the gas must be decreased to avoid elutration of the smaller particles and the chamber length must be increased to provide adequate residence time for heat

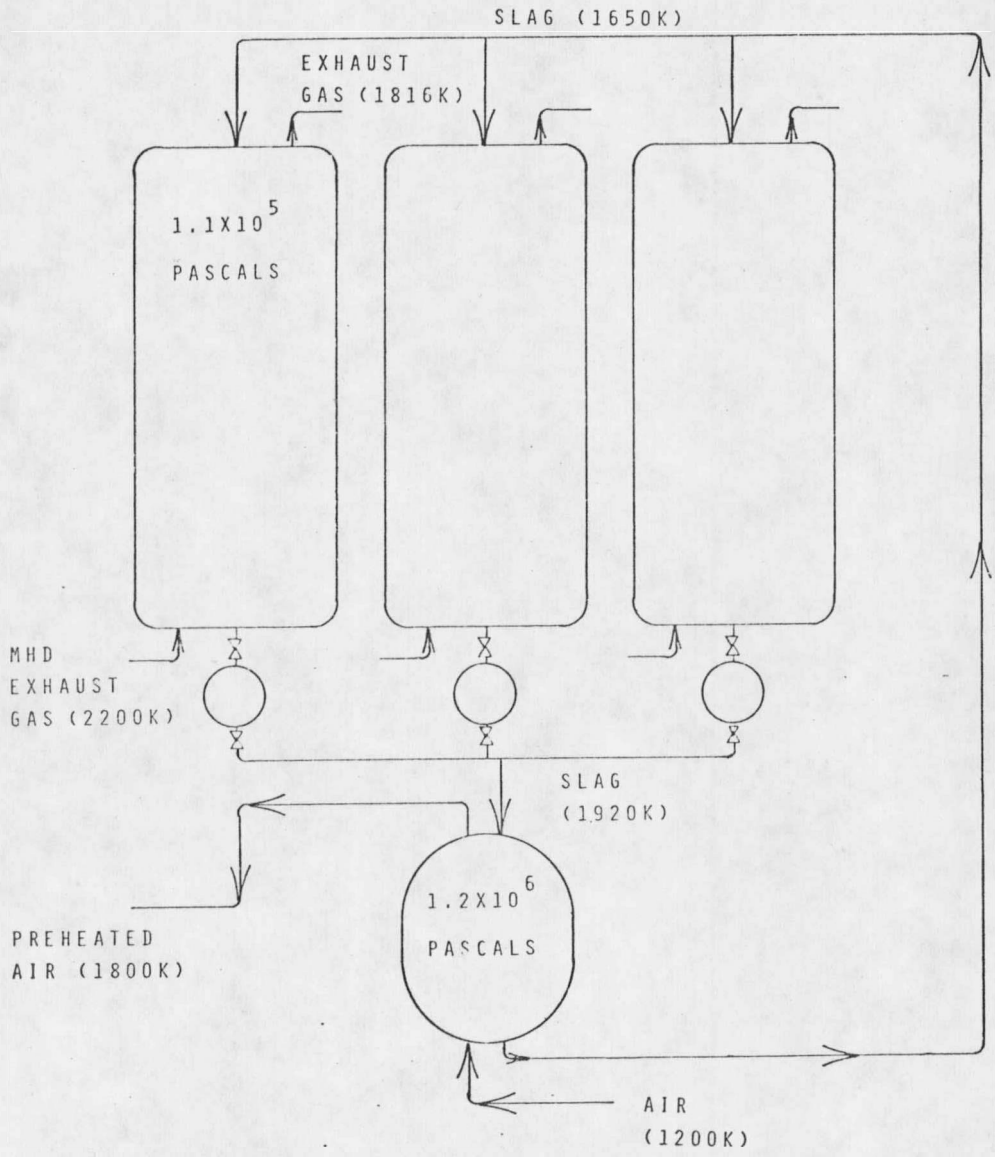

FIGURE 1.1 FALLING LIQUID SLAG DROPLET AIR PREHEATER

transfer to or from the larger droplets. Therefore, the feasibility of a falling bed heat exchanger using liquid slag as the bed material is dependent on a narrow dispersion of the droplet diameters.

Mono-disperse sprays have been achieved by vibration induced atomization. With this method the droplets are formed by disturbing a liquid capillary jet by either vibration (7, 8) or with external sound pressure waves (9, 10). Experimental data has shown that drops uniform in diameter to within five percent of the mean can be obtained using liquids as inviscid as water and as viscous as glycerin.

The concept of the above described droplet generator and the falling bed heat exchanger using liquid slag as the heat transfer media are combined in the following preheater design. It is shown that narrow droplet size distributions obtainable with the droplet generator can render an efficient and compact directly fired, high temperature preheater for open cycle fossil fueled MHD applications. Some of the off design operational characteristics are also considered.

CHAPTER II

ANALYTICAL MODEL

The differential equations for the heat transfer within the heat exchanger were obtained from basic principles.

Radiative Transfer

Radiative energy exchange between any two droplets in the chamber depends upon the solid angle subtended by one droplet as viewed from the other. Therefore, it is necessary to derive an expression for the shadowing effect of the particles.

Consider an incremental sphere of radius ℓ and thickness $d\ell$ centered about a droplet of diameter d_i as shown in Figure 2.1. Assume the sphere is occupied by droplets of diameter d_m located randomly with an average number density n. Let $\Omega(\ell)$ represent the total solid angle subtended by all of the droplets within the sphere. The fraction of solid angle not yet shadowed by these droplets is

$$f(\ell) = (4\pi - \Omega(\ell))/4\pi \qquad 2.01$$

Then the solid angle subtended by the droplets within the incremental sphere is

$$d\Omega(\ell) = \left(\frac{n\pi d_m^2}{4\ell^2}\right)(4\pi\ell^2 d\ell)\, f(\ell) \qquad 2.02$$

This yields the differential equation

$$\frac{d\Omega}{d\ell} + \frac{n\pi d_m^2}{4}\,\Omega(\ell) - \pi^2 d_m^2\, n = 0 \qquad 2.03$$

With the boundary condition

$$\Omega(o) = 0 \ ,$$

the solution is

$$\Omega(\ell) = 4\pi(1-e^{-n\pi d_m^2 \ell/4}) \qquad 2.04$$

Therefore,

$$f(\ell) = e^{-n\pi d_m^2 \ell/4} \qquad 2.05$$

To derive the equations for the net radiation it was assumed that the droplets are black bodies. It was further assumed that the droplets form an optically dense cloud and the radiation penetration distance is small compared with the distance over which significant temperature changes occur. Thus the gas was considered transparent. After the equations were solved, this latter assumption was checked and the absorption by the gases was found to be small (11). The radiative transfer from a droplet of diameter d_m in the annulus to the droplet of diameter d_i as shown in Figure 2.2 is

$$Qr_{2\to1} = \frac{i_b \pi^2 d_i^2 d_m^2}{16\ell^2} \quad f(\ell) \qquad 2.06$$

where

$$i_b = \sigma T_{sm}^4/\pi \qquad 2.07$$

and

$$\ell^2 = x^2 + r^2 \qquad 2.08$$

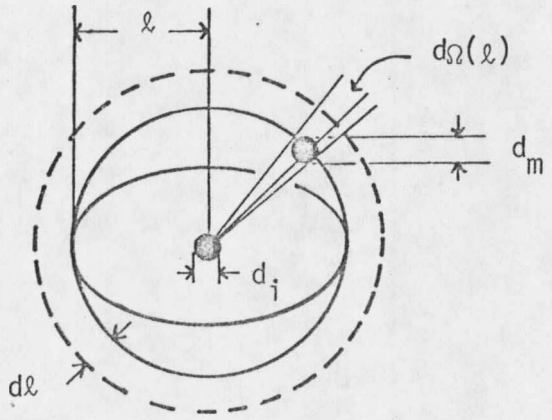

FIGURE 2.1 INCREMENTAL SPHERE FOR DERIVATION OF SHADOWING EFFECT

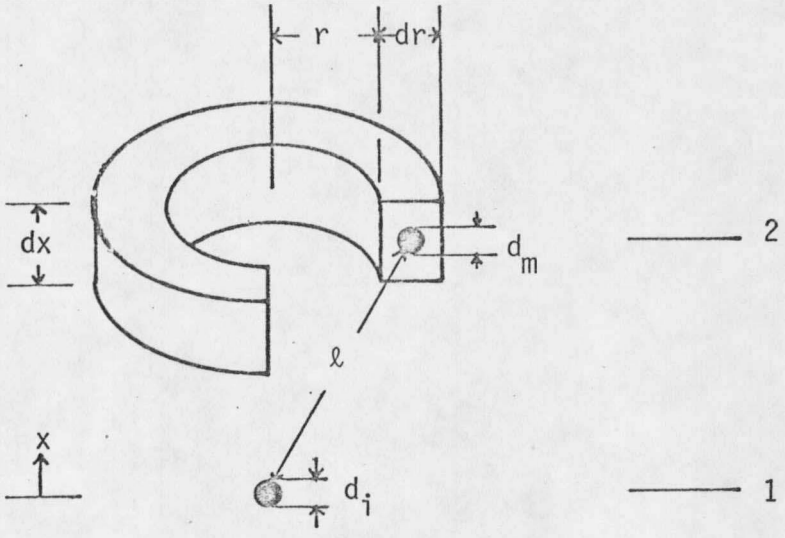

FIGURE 2.2 INCREMENTAL ANNULUS FOR DERIVATION OF RADIATIVE TRANSFER

The total radiative transfer from all of the droplets is then

$$Qr_{2\to1} = \frac{n\sigma\pi^2 d_i^{\,2} d_m^{\,2}}{8} \int_{x=-\infty}^{x=\infty} T_{sm}^{\,4}(x) \left\{ \int_{r=o}^{r=\infty} \frac{re^{-\frac{1}{4}n\pi d_m^{\,2}(x^2+r^2)^{\frac{1}{2}}}}{x^2+r^2}\, dr \right\} dx \qquad 2.09$$

Integrating with respect to r yields

$$Qr_{2\to1} = \frac{n\sigma\pi^2 d_i^{\,2} d_m^{\,2}}{8} \int_{x=-\infty}^{x=\infty} T_{sm}^{\,4}(x)\, E_1(|\alpha x|)dx \qquad 2.10$$

where

$$\alpha = 1/4\ n\pi d_m^{\,2} \qquad 2.11$$

and $E_1(x)$ is the first exponential integral function

$$E_1(x) = \int_x^\infty 1/t \left(e^{-t}\ dt\right) \qquad 2.12$$

The integration of equation (2.10) requires the temperature of the slag droplets to be specified as a function of x. Since this is not known, a Taylor's series expansion about x=0 truncated after the first four terms of the series is employed.

$$T_{sm}^{\,4} = g(x) \simeq g(o) + xg'(o) + \frac{x^2}{2}\, g''(o) + \frac{x^3}{6}\, g'''(o) \qquad 2.13$$

Substituting (2.13) into (2.10) and using the relationship

$$\int_{-\infty}^{\infty} x^n E_1(|x|)\,d_x = \begin{cases} 0, & n \text{ odd} \\ 2\int_0^{\infty} x^n E_1(x)\,dx, & n \text{ even} \end{cases} \qquad 2.14$$

yields

$$Qr_{2\to1} = \frac{n\sigma\pi^2 d_i^{\,2} d_m^{\,2}}{4} \int_0^{\infty} \left[g(o)E_1(\alpha x) + \tfrac{1}{2}x^2 g''(o)E_1(\alpha x) \right] dx \qquad 2.15$$

Integration of equation (2.15) gives

$$Qr_{2\to1} = \sigma\pi d_i^{\,2} T_{sm}^{\,4} + \frac{16\sigma d_i^{\,2}}{3\pi n^2 d_m^{\,4}} \frac{d^2(T_{sm}^{\,4})}{dx^2} \qquad 2.16$$

Since the rate of thermal emission from the droplet d_i is

$$Qr_1 = \sigma\pi d_i^{\,2} T_{si}^{\,4} \quad , \qquad 2.17$$

the net radiative heating rate of the droplet is

$$Qr_{net} = \frac{16\sigma d_i^{\,2}}{3\pi n^2 d_m^{\,4}} \frac{d^2(T_{sm}^{\,4})}{dx^2} + \sigma\pi d_i^{\,2}(T_{sm}^{\,4} - T_{si}^{\,4}) \qquad 2.18$$

Equation (2.18) represents the net radiative heating of a droplet of diameter d_i by the surrounding droplets of diameter d_m. This is included in the energy balance for the falling droplets. When the energy balance for the control volume is applied, it is necessary to

represent the net radiative heat flux. If the average mean free path of a photon emitted by a droplet is small compared with the distance over which significant temperature changes occur, then the net radiative heat flux is obtained by use of the Rosseland diffusion equation (12).

$$q_r = \frac{-16\sigma T^3}{3a_r} \quad \frac{dT}{dx} \qquad 2.19$$

where a_r is the Rosseland mean absorption coefficient. In this case a_r would equal α defined in equation (2.11) and T the local mean slag temperature. Then

$$q_r = - \frac{64\sigma T_{sm}^3}{3\pi d_m^2 n} \quad \frac{d\ (T_{sm})}{dx} \qquad 2.20$$

Equation (2.20) represents the radiative diffusion through the slag droplet cloud.

Droplet Energy Balance

Fine (13) has found the thermal diffusivity of slags similar to coal slag at temperatures of 1600K to be on the order of $5 \times 10^{-7} (m^2/sec)$. The resulting Biot modulus for the diameters considered is between 0.3 and 0.8. Based on these low Biot numbers and the internal mixing within the droplet, an isothermal sphere is assumed.

Consider a droplet of diameter d_i falling through a counterflow of gas as shown in Figure 2.3. Then

$$\rho_s\ c_{si}\ (\frac{\pi d_i^3}{6}) \quad \frac{d(T_{si})}{dt} = Q_{cov} + Qr_{net} \qquad 2.21$$

but

$$\frac{d(T_{si})}{dt} = \frac{d(T_{si})}{dx}\,\frac{dx}{dt} = \frac{d(T_{si})}{dx}\,V_{si} \qquad 2.22$$

and

$$Q_{cov} = \pi h_i d_i^{\,2}\,(T_g - T_{si}) \qquad 2.23$$

$$n = \frac{24\,\dot{m}_s}{\pi^2 V_{sm}\rho_s d_m^{\,3} D_{in}^{\,2}} \qquad 2.24$$

Combining equations (2.21) through (2.24) and (2.18)

$$\frac{dT_{si}}{dx} = \frac{6h_i(T_g - T_{si})}{\rho_s c_{si} d_i V_{si}} + \frac{\sigma\rho_s(\pi V_{sm} d_m D_{in}^{\,2})^2}{18 c_{si} d_i V_{si} \dot{m}_s^{\,2}}\,\frac{d^2(T_{sm}^{\,4})}{dx^2} +$$

$$\frac{6\sigma}{\rho_s c_{si} d_i V_{si}}\,(T_{sm}^{\,4} - T_{si}^{\,4}) \qquad 2.25$$

Equation (2.25) represents the derivative with respect to position of the temperature of the particles of diameter d_i as they fall through the chamber. For the idealized case of one droplet diameter (mono-disperse) there is one equation of this form, and d_i equals d_m, T_{si} equals T_{sm}, etc. When there is dispersion in the droplet diameters, this is accounted for by letting d_i denote the diameter of the droplets of the i^{th} discrete size; i=1 denotes the smallest droplets and i=N denotes the largest droplets. Thus, there are N equations of the above form

(one for each discrete size).

Control Volume Energy Balance

The equation for the heat exchange between the droplets and the gas is derived using the control volume shown in Figure 2.4. The heat loss from the walls per unit area is represented by q_w. The radiative diffusion term, q_r, is presented in equation (2.20). An energy balance for the control volume yields

$$\sum_{i=1}^{N} (\dot{m}_{si} c_{si} T_{si}|_x - \dot{m}_{si} c_{si} T_{si}|_{x+\Delta x}) + \tfrac{1}{4}\pi D_{in}^2 (q_r|_x - q_r|_{x+\Delta x})$$

$$+ (c_g \dot{m}_g T_g|_{x+\Delta x} - c_g \dot{m}_g T_g|_x) - q_w \pi D_o \Delta x = 0 \qquad 2.26$$

Rearranging and using equation (2.20)

$$\frac{dT_g}{dx} = \sum_{i=1}^{N} \frac{\dot{m}_{si} c_{si}}{\dot{m}_g c_g} \frac{d(T_{si})}{dx} - \frac{2\pi^2 \sigma \rho_s d_m D_{in}^4 V_{sm}}{9 \dot{m}_s \dot{m}_g c_g}$$

$$\frac{d}{dx}\left(T_{sm}^3 \frac{d(T_{sm})}{dx}\right) + \frac{q_w \pi D_o}{c_g \dot{m}_g} \qquad 2.27$$

Heat Loss From the Wall

Before the heat loss can be calculated, the insulation material and thickness has to be determined. The eight types of ceramic insulation considered are listed in Table 2.1. The inner wall

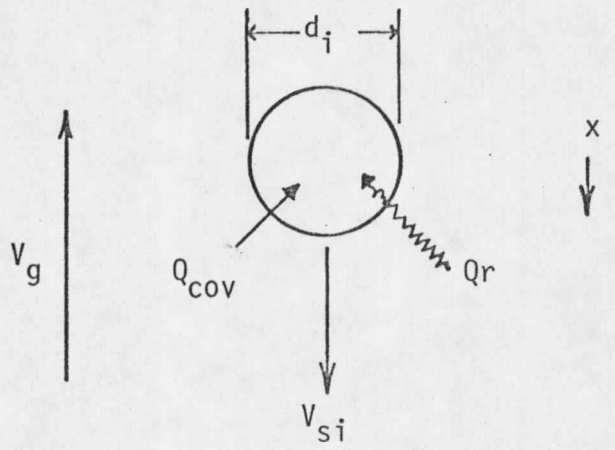

FIGURE 2.3 DROPLET ENERGY BALANCE

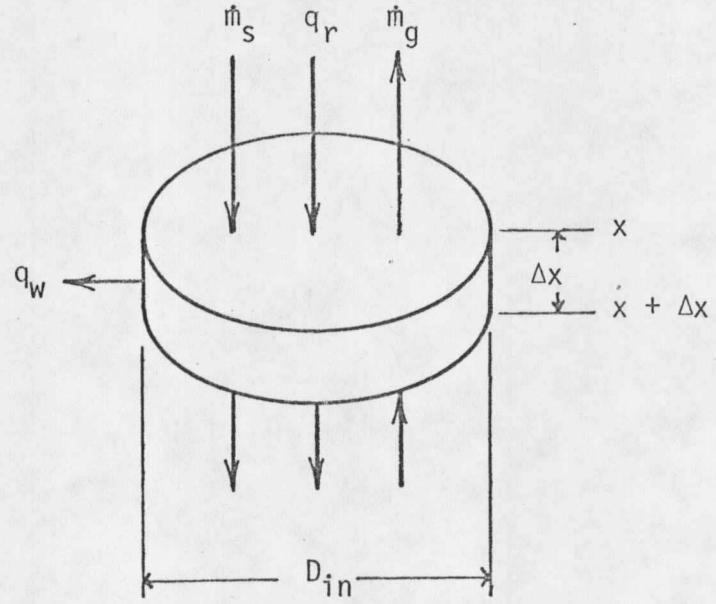

FIGURE 2.4 CONTROL VOLUME FOR ENERGY BALANCE

TABLE 2.1 PROPERTIES OF THE INSULATING MATERIALS

Manufacturer	Type	Thermal Conductivity (j/m-sec-K)	Upper Temperature Limit (K)	Standard Size (cm)
Norton	AN-599	1.290	2140	7.62
Johns-Manville	JM-3200	0.503	2030	11.43
Johns-Manville	JM-3000	0.475	1920	11.43
Johns-Manville	JM-2800	0.424	1810	11.43
Johns-Manville	JM-2600	0.338	1700	11.43
Johns-Manville	JM-2500	0.308	1640	11.43
Johns-Manville	JM-2300	0.144	1530	11.43
Johns-Manville	Cerawool	0.078	1140	5.08

temperature is assumed to be equal to the local mean slag droplet temperature and the outer wall is specified at 370K. Because of the corrosive environment within the exchanger, Norton AN-599 bubble alumina brick is used as the first layer of insulation. This layer is to be 7.62 cm thick. The outer layer of insulating material, Johns-Manville Cerawool, is chosen because of its lower thermal conductivity and its ability to absorb any condensation which might occur on the inner wall of the enclosing pressure vessel. This layer is to be 5.08 cm thick. Respective thicknesses of the remaining insulations are chosen by a computer trial and error technique as outlined below. Thermal resistance of the metal pressure vessel is ignored.

To determine the convective film coefficient on the outside wall, natural convection is assumed. For an ambient air temperature of 295K and a characteristic length of eight meters the Grashof number Prandtl number product is

$$GrPr = 2.5 \times 10^{12}$$

Since this is in the turbulent range for natural convection, the resulting Nusselt number is

$$Nu = .13(GrPr)^{.333} \qquad (14)$$

Then

$$h = .13 \left(\frac{c_a \beta_a (T_o - T_a) \rho_a^2}{k_a \mu_a}\right)^{.333} k_a \qquad 2.28$$

The optimizing criterion for determining the insulation thicknesses is the outer chamber diameter; the idea being to maximize the thickness of the lower conductivity materials and thus minimize the outer diameter. The design constraints are to keep the temperatures at the interfaces within the limits of the respective insulations. The computer routine that chooses and sizes the respective insulations begins by trying only the high thermal resistance material between the specified inner and outer layers. If the interface temperatures are too high, successive layers of the lower resistant insulations are added until the interface temperatures are within the limits of the respective insulations.

Consider the case where only one type of insulating material between the specified outer and inner layers of insulations is used as shown in Figure 2.5. From the solution of the conduction equations for radial heat transfer with cylindrical symmetry

$$T_2 = T_{in} - \frac{R_o(T_o-T_a)h\ln(R_2/R_1)}{k_1} \qquad 2.29$$

$$T_3 = T_2 - \frac{R_o(T_o-T_a)h\ln(R_3/R_2)}{k_2} \qquad 2.30$$

Equating the heat in and out of each face

$$R_3 = R_2\, e^{(T_2 - T_3)k_3/(T_o-T_a)hR_o} \qquad 2.31$$

These are solved by use of successive substitution and the interface temperatures are checked against the upper temperature limit specifications of the insulation materials. If these are too high, a layer of the next higher rated temperature insulating material is added, and the interface temperatures are calculated and checked. Each layer of insulation added is 11.4 cm thick--the size commercially available. This method is repeated until all of the temperatures were within the limits of the respective materials.

After these steps are completed, another check is made to see if any of the interface temperatures are low enough to replace a layer of insulation with the next lower conductive insulation. For instance, the above method could result with a layer of JM-2300, a layer of JM-2500, and a layer of JM-2600, when the temperature between the JM-2500 and the JM-2600 is low enough to replace the JM-2500 with JM-2300.

Once the insulation sizes are determined, the heat flux term is calculated using an overall heat transfer coefficient

$$q_w = H(T_{in} - T_a)$$

where q_w represents the heat loss from the wall as used in Equation (2.27) and

$$H = 1/\left(\frac{1}{h} + \sum_i \frac{R_o \ln(R_{i+1}/R_i)}{k_i}\right) \quad (15) \qquad 2.32$$

Falling Droplet Dynamics

The expression for the dynamics of a spherical droplet of diameter d_i falling through a counterflow of gas is derived by use of the free body diagram illustrated in Figure 2.6. Ignoring the buoyant force ($\rho_g/\rho_s << 1$)

$$\frac{dV_{si}}{dx} = \frac{a}{V_{si}} - \frac{3}{4} \frac{C_D \rho_g V_{ri}^2}{d_i \rho_s V_{si}} \qquad 2.33$$

As with equation (2.25), there are N equations of this form (one equation for each discrete droplet size).

The diameter of the chamber depends on the terminal velocity of the smallest particle. The terminal velocity is calculated from the expression

$$V_{term} = \left(\frac{4a\rho_s d_i}{3C_D \rho_g}\right)^{\frac{1}{2}} \qquad 2.34$$

Dimensionless Relations

To facilitate ease of solution and use of dimensionless emperical correlations, the above equations were normalized using the following parameters

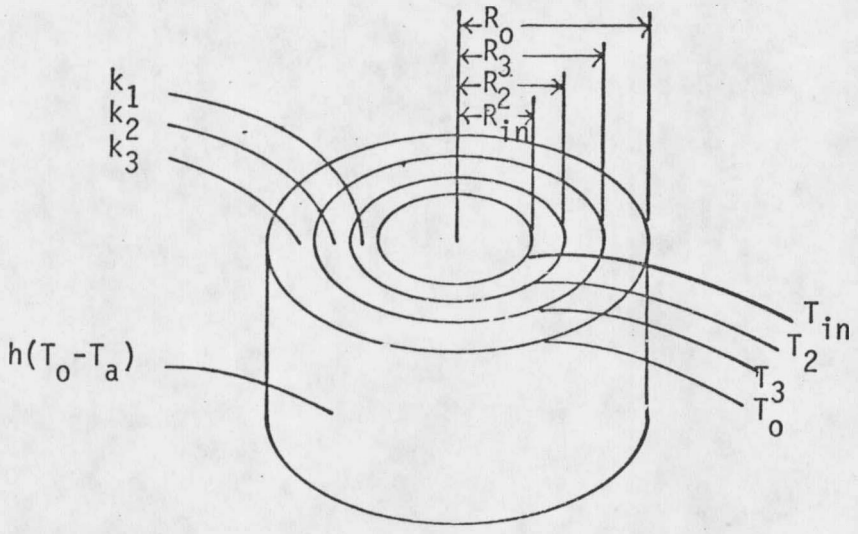

FIGURE 2.5 GEOMETRY FOR THE CASE OF THREE LAYERS OF INSULATION

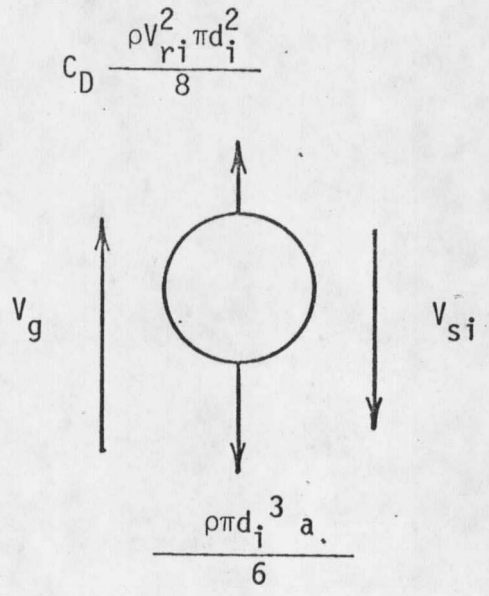

FIGURE 2.6 DROPLET FREE BODY DIAGRAM

$$\phi_g = \frac{T_g - T_{1,g}}{T_{2,g} - T_{1,g}}$$

$$\phi_{si} = T_{si}/T_{1,s}$$

$$\eta = x/D_o$$

$$U_i = V_{ri}/V_{1,r}$$

$$U_m = V_{rm}/V_{1,r}$$

$$U_g = V_g/V_{1,r}$$

$$\rho^* = \rho_s/\rho_g$$

$$c_i^* = c_{si}/c_g$$

$$d_i^* = d_i/D_o$$

$$\dot{m}_i^* = \dot{m}_{si}/\dot{m}_g$$

$$Re_i = \frac{\rho_g V_{ri} d_i}{\mu_g} = \text{Reynolds Number}$$

$$Nu_i = \frac{h_i d_i}{k_g} = \text{Nusselt Number}$$

$$Pr = \frac{\mu_g c_g}{k_g} = \text{Prandtl Number}$$

Equations (2.25), (2.27), and (2.33) transform respectively into the following:

$$\frac{d\phi_{si}}{d\eta} = \frac{6Nu_i\, U_i\, (\Psi 1\phi_g + \Psi 2 - \phi_{si})}{Re_i\, Pr\, \rho^*\, c_i^*\, d_i^*\, (U_i - U_g)} +$$

$$\Psi 3_i\, \frac{d^2(\phi_{sm}^4)}{d\eta^2} + \Psi 4_i\, (\phi_{sm}^4 - \phi_{si}^4) \qquad 2.35$$

$$\frac{d\phi_g}{d\eta} = (1/\Psi 1)\left(\sum_{i=1}^{N} c_i^*\, \dot{m}_i^*\, \frac{d\phi_{si}}{d\eta}\right) - \Psi 5\, \frac{d^2\phi_{sm}}{d\eta^2} + \Psi 6 \qquad 2.36$$

$$\frac{dU_i}{d\eta} = \frac{\Psi 7}{(U_i - U_g)} - \frac{3c_D U_i^2}{4\rho^* d_i^* (U_i - U_g)} + \Psi 8\, \frac{d\phi_g}{d\eta} \qquad 2.37$$

where

$$\Psi 1 = (T_{2,g} - T_{1,g})/T_{1,s}$$

$$\Psi 2 = T_{1,g}/T_{1,s}$$

$$\Psi 3_i = \frac{\sigma\rho_s(\pi V_{sm} d_m D_{in}^2)^2 T_{1,s}^3}{18\, c_{si} d_i V_{si} \dot{m}_s^2 D_o}$$

$$\Psi 4_i = \frac{6\sigma D_o T_{1,s}^3}{\rho_s c_{si} d_i V_{si}}$$

$$\Psi 5 = \frac{\pi^2 \sigma \rho_s d_m D_{in}^4 V_{sm} T_{1,s}^4}{18\, D_o\, \dot{m}_s\, \dot{m}_g\, c_g (T_{2,g} - T_{1,g})}$$

$$\Psi 6 = \frac{q_w \pi D_o^2}{c_g \dot{m}_g (T_{2,g} - T_{1,g})}$$

$$\Psi 7 = aD_o / V_{1,r}^2$$

$$\Psi 8 = \frac{\dot{m}_g R (T_{2,g} - T_{1,g})}{P\, A\, V_{1,r}}$$

The values for the Nusselt number were correlated from published data as

$$Nu_i = .29 Re_i^{.630} Pr^{.333} \qquad (15) \qquad 2.38$$

The drag coefficient was determined from the Reynolds number

$$C_D = \begin{cases} 18.5/Re^{.600} & Re<200 \\ 5.74/Re^{.372} & 200 \leq Re \leq 1000 \\ 0.44 & Re > 1000 \end{cases} \qquad (16) \qquad 2.39$$

The above parameters and equations apply to the top chamber but would be identical for the lower chamber with the exception that T_1, T_2, V_1 and V_2 would be replaced by T_3, T_4, V_3 and V_4 respectively.

Method of Solution

The non-linear set of ordinary differential equations (2.35) through (2.37) represent a boundary value system with one known boundary. Although the boundary values are known at x=L, L itselt is unknown. Assuming the equations are well behaved, the system can be solved by an initial value numerical method. An energy balance of the entire heat exchanger system is used to find the temperatures at the top of the chambers and the mass flow rates. Thus (2N+1) initial values are known, leaving only one to be approximated--the first derivative of the mean slag temperature.

The problem arises from the form of equation (2.25). For the mean slag temperature the equation is

$$\frac{d(T_{sm})}{dx} = C1\ (T_g - T_{sm}) + C2\ \frac{d^2(T_{sm}^4)}{dx}$$

where C1 and C2 represent the variable coefficients. If the system is solved with the second term to the right of the equal sign equal to zero, the temperature profiles are nearly linear. The addition of the second term renders the temperature solution, and its derivatives, exponential in nature and extremely sensitive to the initial value

approximation and numerical truncation error. Any slight error will compound itself exponentially and dominate the equations, rendering the solution meaningless.

The second derivative term represents a portion of the radiative transfer while the first term to the right of the equal sign represents the convective transfer. Defining ε as the ratio of these two terms and employing an order of magnitude analysis yields

$$\varepsilon = \frac{C2 \ \frac{d^2(T_{sm}{}^4)}{dx^2}}{C1 \ (T_g - T_{sm})} = \frac{C2\left(12T_{sm}{}^2 \ (\frac{dT_{sm}}{dx})^2 + 4 \ T_{sm}{}^3 \ \frac{d^2(T_{sm})}{dx^2}\right)}{C1 \ (T_g - T_{sm})}$$

with

$$\frac{d^2T_{sm}}{dx^2} \simeq \frac{\Delta T}{L^2}$$

and

$$\frac{dT_{sm}}{dx} \simeq \frac{\Delta T}{L}$$

For the upper chamber using quantities from a numerical solution obtained with the radiative term neglected results in

$$\varepsilon \simeq 0.030$$

and for the lower chamber

$$\varepsilon \simeq 0.002$$

Since these ratios are much less than one, the radiation term is small in comparison to the convection term. Therefore, the radiation

second derivative term in equation (2.35) was ignored in order to solve the equations. This is not to say that thermal radiation is ignored in the analysis; but rather, the second derivative term in equation (2.18) was dropped.

The initial conditions at the top of the chamber are

$$\phi_{si} = U_i = 1$$

$$\phi_g = 0$$

The initial value for the second derivative term in equation (2.36) had to be approximated in order to initiate the numerical iteration. Since this term had little effect on the results (less than one percent) the approximation did not have to be very accurate.

A fourth order Runge-Kutta integration technique was employed to solve the system of equations. In the bottom chamber the length was determined by integrating until ϕ_g equaled one, while in the top chamber the predetermined slag exit temperature was used as the parameter to determine the length.

Error analysis for higher order Runge-Kutta schemes is very difficult or impossible to implement for systems of nonlinear differential equations of this type (17). To check the convergence and stability several different step sizes were used. No apparent problems arose.

CHAPTER III

DROPLET FORMATION

A critical element in the design of a falling bed counterflow heat exchanger is control of the dispersion of the droplet diameters. To prevent any of the particles from being blown out of the top, the velocity of the gas through the chamber must be limited by the terminal velocity of the smallest particles. If the droplet sizes are characterized by a wide dispersion, the larger particles will fall much faster than the smaller ones and the length of the chamber will become unfeasibly large. For example, the particle size distribution obtained from Heywood and Womack (6) using a twin jet atomizer would require chamber lengths in excess of 100 meters for an MHD preheater. Figure 3.1 further illustrates the effect of particle dispersion on the chamber dimensions. One conceptual solution to this problem is the formation of the slag droplets by vibration atomization.

In the proposed atomizer, referred to as a drop generator, the liquid is forced through a capillary which is vibrated at a predetermined frequency to produce uniformly sized drops. This technique has been used primarily in research applications such as combustion (8) and drop coalescence studies (18). The first quantitative analysis of liquid jet disintegration was made in 1878 by Lord Rayleigh (19). His results, which are applicable to an inviscid fluid without any aerodynamic forces acting on it, showed that the frequency for maximum instability, and hence the optimum frequency for uniformly sized drops,

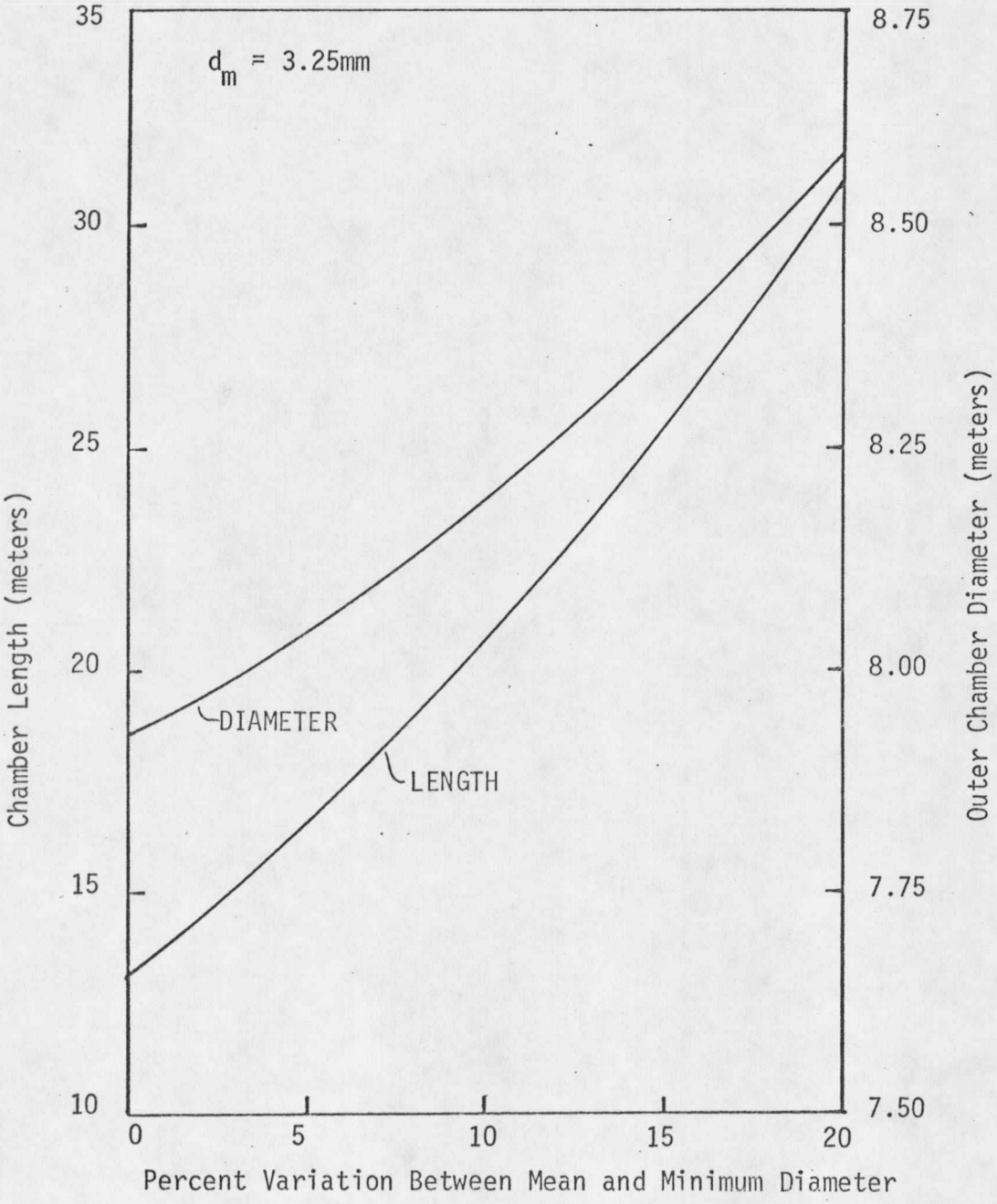

FIGURE 3.1 EFFECT OF PARTICLE DISPERSION ON LENGTH AND DIAMETER OF THE UPPER CHAMBER FOR A 3000MWt MHD FACILITY

is given by

$$F_{opt} = V_j/4.508\ D_j \qquad 3.01$$

This analysis was extended by Levich (20) to include the effects of fluid viscosity and surface tension forces resulting in

$$F_{opt} = \left(\frac{V_j}{13}\right)\left(\frac{8\ \sigma_s\ \rho}{\mu^2\ D_j^3}\right)^{\frac{1}{4}} \qquad 3.02$$

The minimum frequency for the formation of nearly uniformly sized drops was determined empirically by Rajogopalan and Tien (7) as

$$F_{min} = 0.4\ F_{opt} \qquad 3.03$$

These same researchers also determined the theoretical expression for the drop size resulting from the jet disintegration

$$d = 1.145\left(\frac{V_j}{F}\right)^{1/3} D_j^{2/3} \qquad 3.04$$

The minimum average velocity in the capillary necessary to form a stable jet, as determined by Lindbald and Schneider (18) is

$$V_{c,min} = \left(\frac{8\ \sigma_s}{\rho D_j}\right)^{\frac{1}{2}} \qquad 3.05$$

Harmon (21) has related the capillary diameter to the free stream jet diameter by

$$D_j = 0.867\ D_c \qquad 3.06$$

The above equations were used to simulate the drop generator for the heat exchanger application. There are two methods of disturbing the liquid jet:

1) Flowing the liquid through capillaries in a plate which is vibrated within a predetermined frequency range
2) Flowing the liquid through capillaries in a stationary plate with the disturbance produced by external sound pressure waves.

Uniformly sized drops (to within five percent of the mean) have been achieved by the first method (7,8). The second method was investigated by Miesse (9) but no size distributions were published.

A major factor in the variation of droplet diameters is the variation in the capillary diameters. The required number of capillaries is in the distributor plate at the chamber top is

$$\text{Number of Capillaries} = \frac{4\,\dot{m}_s}{\rho_s V_c\,\pi\,D_{c,m}^{\,2}} \qquad 3.07$$

Because of the high temperatures, extruded ceramic tubing is suggested for the capillaries. The standard tolerances for this tubing with inside diameters ranging from 1.3×10^{-2} to 1.3×10^{-3} meters is ±3% or 1.3×10^{-4} meters, whichever is greater. These tolerances were used to find the minimum capillary diameter for a specified mean capillary diameter. For laminar flow the pressure drop across the smallest capillary is given by

$$\frac{\Delta P}{\ell_c} = \frac{32\mu_s \, V_{c,\,min}}{\pi \, D_{c,min}^{\,2}} \qquad 3.08$$

where $V_{c,min}$ is the minimum velocity required to form a jet in the smallest capillary. Since the capillary lengths are equal, the velocity in the mean capillary diameter is given by

$$V_{c,m} = \frac{V_{c,min} \; D_{c,m}^{\,2}}{D_{c,min}^{\,2}} \qquad 3.09$$

The optimum operating frequency is calculated using equation (3.02). From equation (3.04) the mean droplet diameter from the smallest capillary and the mean droplet diameter from the mean capillary are obtained. Assuming the droplet diameters from any capillary vary within 5% of the mean droplet diameter of that capillary, the smallest droplet within the exchanger is calculated from the mean droplet diameter of the smallest capillary. That is

$$d_{min} = .95 \; d_{m,min}$$

$$d_m = d_{m,m}$$

The capillary diameters and the droplet dispersions are assumed to follow a normal distribution. In order to calculate the standard deviation, it was further assumed that 99% of all of the droplets within the chamber are within the diameter range as calculated above. This results in a standard deviation of

$$s_d = \frac{d_m - d_{min}}{2.576} \qquad (22) \qquad 3.10$$

The frequency function for the particle distribution was then generated by

$$f(d_i) = \frac{1}{s_d\sqrt{2\pi}} e^{-(d_i-d_m)^2/2s_d^2} \qquad 3.11$$

For the discrete number of droplet sizes as modeled in the computer code the respective number fractions were obtained by integration of the frequency function.

CHAPTER IV

RESULTS

The equations presented in Chapter II and Chapter III were applied to the design of an MHD air preheater system. The computer program outlined in Appendix II was used to numerically integrate the equations. The operating conditions for the 3000 MW thermal open cycle facility considered were similar to those of the ECAS Base Case One Open Cycle study (23) but with higher operating temperatures. Higher temperatures increase the thermal efficiency of the plant. The pressure at the ingress of the channel was also higher than that of the ECAS study; this being appropriate for the higher operating temperatures (24). After the chambers were sized using these operating conditions, partial load operation was studied.

Full Load Design

The diameters of the chambers are dependent on the mass flow rate of the gas through the chamber and the terminal velocity of the smallest droplet. In order to keep these diameters reasonable, it was necessary to use three sets of preheaters. Each of these sets consists of three upper chambers and one lower chamber as shown in Figure 1.1. The parameters $T_{2,g}$, $T_{3,g}$, $T_{4,g}$, $\dot{m}_g$, and $\dot{m}_s$ were specified. Chamber length, slag mass flow rate, and pressure drop through the capillaries were the design criteria while the slag temperatures, capillary diameter and disturbance frequency were the variable design parameters.

The effects of the operating slag temperatures on the design criteria are shown in Figure 4.1, Figure 4.2, and Figure 4.3. Figure 4.1 was obtained by arbitrarily choosing a capillary diameter of 2mm and the operating frequency at the corresponding optimum disturbance frequency. The mass flow rate of the slag was obtained by an energy balance on the lower chamber with the heat loss from the chamber walls assumed negligible. It was also assumed that the heat loss from the piping that transports the slag from one heat transfer chamber to another was negligible; that is, $T_{1,s}$ equals $T_{4,s}$ and $T_{2,s}$ equals $T_{3,s}$. The exhaust gas temperature at the exit of the upper exchanger was calculated from an energy balance for the entire system and checked to be sure that it was higher than the dew point of the potassium sulfate (about 1600 K).

Decreasing the temperature variation of the slag increases the slag mass flow rate required and decreases the aggregate chamber length. (The aggregate length refers to the length of one upper chamber plus the length of the lower chamber). In order to keep the lengths reasonable without the flow rate of the slag becoming excessive, the total temperature difference for the slag media was chosen at 270K. Since the slag becomes very viscous at lower temperatures, the pressure drop through the capillaries at the top of the upper chamber is critical. Therefore, the lowest working slag temperature was chosen at 1650K. Though the pressure drop would be less if a higher temperature were

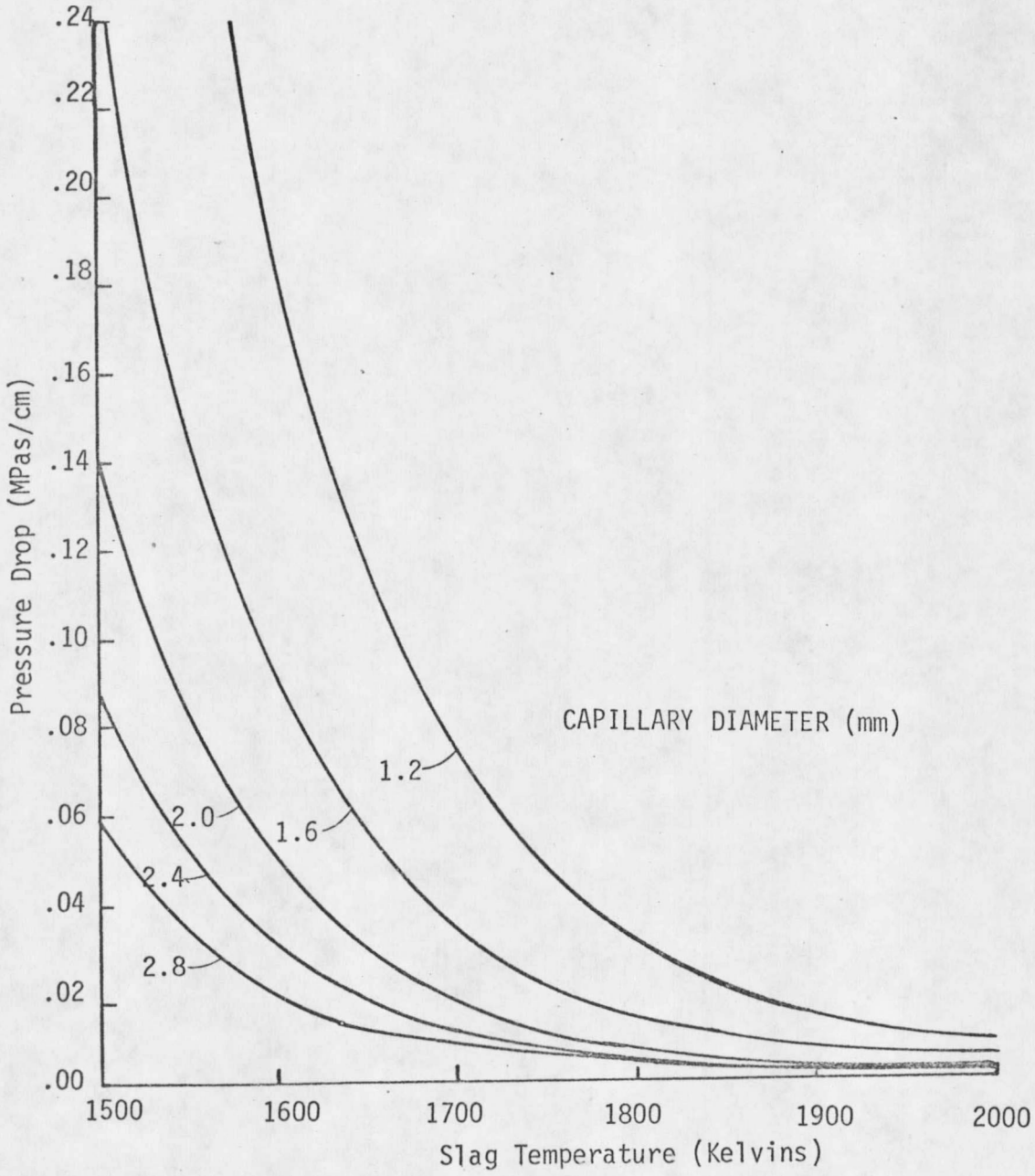

FIGURE 4.1 EFFECT OF SLAG TEMPERATURE AND CAPILLARY DIAMETER ON THE PRESSURE DROP THROUGH THE CAPILLARY